Spatial solitons and instabilities of light beams in a three-level atomic medium with a standing-wave control field

Chao Hang,[1,2] V. V. Konotop,[1,3] and Guoxiang Huang[2,4]
[1]*Centro de Física Teórica e Computacional, Universidade de Lisboa, Complexo Interdisciplinar, Avenida Professor Gama Pinto 2, Lisboa 1649-003, Portugal*
[2]*Department of Physics and State Key Laboratory of Precision Spectroscopy, East China Normal University, Shanghai 200062, China*
[3]*Departamento de Física, Faculdade de Ciências, Universidade de Lisboa, Campo Grande, Ed. C8, Piso 6, Lisboa 1749-016, Portugal*
[4]*Department of Physics, Zhejiang Normal University, Jinhua, 321004 Zhejiang, China*
(Received 13 November 2008; published 17 March 2009)

We consider propagation of a weakly nonlinear probe light beam in a resonant three-level atomic system where an optical lattice is induced by a standing-wave control field and conditions for electromagnetically induced transparency are created. We employ a unified theory to solve the respective nonlinear system of equations in various regimes and investigate formation of spatial optical solitons and instabilities, both analytically and numerically. We show that the effect of the lattice is twofold. On the one hand it allows one to reduce the probe beam intensity necessary for observation of nonlinear effects until the level of one-photon energy, and on the other hand the lattice allows for implementation of different dynamical regimes either by simple manipulation of its parameters or by varying one- and two-photon detunings or by changing the geometry of the incident probe beam.

DOI: 10.1103/PhysRevA.79.033826 PACS number(s): 42.65.Tg, 05.45.Yv, 42.50.Gy

I. INTRODUCTION

Solitons are of particular interest due to their practical applications in optical information processing and transmission [1]. Most of optical solitons are produced in passive media, such as glass-based optical fibers, in which far-off-resonance excitation schemes are generally employed in order to avoid uncontrollable optical attenuation and distortion. A drawback of such systems is that their nonlinear effects are usually very weak and hence either very high light intensities or very long optical paths are required for formation of solitons.

Different situation is observed in resonant media allowing for the phenomenon called electromagnetically induced transparency (EIT), which recently received a great deal of attention [2]. When the conditions for the EIT are created, application of a strong resonant control field to an opaque medium makes it transparent to a weak probe field. Due to the atomic coherence and interference induced by the control field, propagation of the weak probe field occurs under significant suppression of losses, reduction in the group velocity [3], and giant enhancement of the Kerr nonlinearity [4]. It has been shown that a new type of optical solitons, termed ultraslow solitons, can exist in such resonant multilevel media under EIT conditions [5]. However, up to now only a few works were dedicated to formation of two-dimensional (2D) spatially localized structures in EIT systems [6,7].

On the other hand, considerable progress has been achieved in the study of propagation of electromagnetic waves in photonic band-gap materials [8]. The main feature of such media is the existence of frequency gaps where linear wave propagation is forbidden. When nonlinearity is taken into account the so-called gap solitons can exist allowing for wave propagation at frequencies belonging to stop gaps. Recently, manipulation of light pulses via a dynamically controlled photonic band-gap structure in EIT media was investigated both theoretically and experimentally [9].

In the present work we propose to employ a resonant optical lattice (OL), created by a standing-wave coupling field, which allows one to achieve two objectives as follows. First, serving as a stabilizing factor, under proper conditions, a lattice allows for further reduction in the probe beam intensity necessary for creation of spatial solitons in a three-level system. In this context, we mention that for sustainability of the stable localized structures reported in Ref. [6], a non-negligible quintic nonlinearity was needed, what has been achieved by using a more sophisticated medium—four-level atomic system. Meantime, in Ref. [7] stronger probe beam intensities resulting in saturable nonlinearity were exploited. In the present paper we show that intensities required due to the optical lattice are 2 orders less than the reported in [7] achieving the level of one-photon energy. Second, the lattice allows for very flexible and manageable implementation of different nonlinear scenarios, including generation of spatial solitons, self-focusing, as well as various types of beam instabilities, in a three-level atomic system under EIT conditions. This is achievable either by changing the geometry and intensity of the control field or by varying one- and/or two-photon detunings or by changing the angle of incidence of the probe laser beam.

Thus, the suggested system appears to be an ideal laboratory for studying nonlinear phenomena in periodic media and to be promising for designing nonlinear band-gap devices working at very low light intensities. While periodic EIT media have already been the subject of studies [9], unlike in the previous works focused mainly on linear properties of periodic media, here we concentrate on effects which stem from enhancement of the Kerr nonlinearity due to the EIT effect, focusing on stable spatial solitons and different types of instabilities of a probe beam.

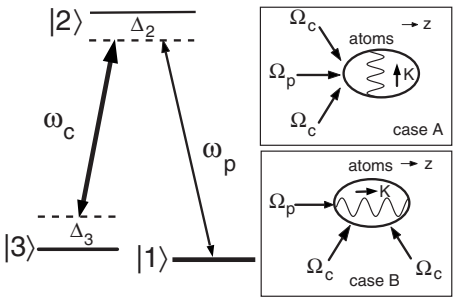

FIG. 1. Schematic representation of the energy level structure of the lifetime-broadened Λ-type atomic system (see the text for the definitions of the notations). Insets show two possible geometries considered in the present study: the probe field propagation direction is orthogonal (the upper panel) and parallel (the lower panel) to the axis of the optical lattice.

The paper is organized as follows. Section II gives a simple description of the model at hand. The polarization of the atomic medium for a weak probe field under the EIT conditions is obtained. In Sec. III, the evolution equation for the slowly varying amplitude of a probe beam is derived for different geometries of the control field. Spatial optical soliton solutions and their stability are investigated analytically and numerically. The main outcomes of our research are briefly summarized in Sec. IV.

II. MODEL

A. Λ-type three-level system

We consider a cold lifetime-broadened three-level Λ-type atomic system, schematically shown in Fig. 1. A weak probe field with the polarization vector $\mathbf{e}_p$, the central frequency ω_p, and the wave vector $\mathbf{k}_p$, i.e., $\mathbf{E}_p(\mathbf{r},t)=\mathbf{e}_p\mathcal{E}_p e^{i(\mathbf{k}_p\cdot\mathbf{r}-\omega_p t)}+\text{c.c.}$, couples the ground, $|1\rangle$, and the excited, $|2\rangle$, states. A strong control field consisting of a pair of counterpropagating waves having the polarization vector $\mathbf{e}_c$, the frequency ω_c, and the wave vectors $\mathbf{k}_c\pm\mathbf{K}$ ($|\mathbf{K}|\ll|\mathbf{k}_c|$), i.e., $\mathbf{E}_c(\mathbf{r},t)=2\mathbf{e}_c\mathcal{E}_c\cos(\mathbf{K}\cdot\mathbf{r})e^{i(\mathbf{k}_c\cdot\mathbf{r}-\omega_c t)}+\text{c.c.}$, couples the states $|2\rangle$ and $|3\rangle$. The total applied electric field has the form $\mathbf{E}(\mathbf{r},t)=\mathbf{E}_p(\mathbf{r},t)+\mathbf{E}_c(\mathbf{r},t)$ and is considered classically. For the sake of convenience, we choose $\mathbf{k}_p=k_p\mathbf{e}_z$, with $\mathbf{e}_z$ being the unit vector along z direction.

The atomic medium is described by the bosonic field operators $\hat{\Psi}_i(\mathbf{r},t)$ $(i=1,2,3)$, satisfying the standard commutation relations: $[\hat{\Psi}_i(\mathbf{r},t),\hat{\Psi}_{i'}^{\dagger}(\mathbf{r}',t)]=\delta_{ii'}\delta(\mathbf{r}-\mathbf{r}')$ and $[\hat{\Psi}_i(\mathbf{r},t),\hat{\Psi}_{i'}(\mathbf{r}',t)]=[\hat{\Psi}_i^{\dagger}(\mathbf{r},t),\hat{\Psi}_{i'}^{\dagger}(\mathbf{r}',t)]=0$. We consider the simplest case of free atoms forming a dilute gas that allows us to neglect the energy of interatomic interactions compared with the interaction energy between the atoms and the light field. Then the Hamiltonian of the system reads $H=\Sigma_{i=1}^{3}H_i+H_{af}$, where H_i $(i=1,2,3)$ are the atomic Hamiltonians,

$$H_i=\int\hat{\Psi}_i^{\dagger}\left(-\frac{\hbar^2}{2M}\nabla^2+\hbar\omega_i\right)\hat{\Psi}_i d^3\mathbf{r}, \tag{1}$$

M is the atomic mass, and $\hbar\omega_i$ is the internal energy of the atoms in state $|i\rangle$. H_{af} describes the interaction of atoms with the electric field, and in the electric-dipole approximation has the form

$$H_{af}=-\int d^3r\hat{\Psi}_2^{\dagger}\hbar\Omega_p(\mathbf{r},t)e^{i(\mathbf{k}_p\cdot\mathbf{r}-\omega_p t)}\hat{\Psi}_1$$
$$-2\int d^3r\hat{\Psi}_2^{\dagger}\hbar\Omega_c(\mathbf{r},t)\cos(\mathbf{K}\cdot\mathbf{r})e^{i(\mathbf{k}_c\cdot\mathbf{r}-\omega_c t)}\hat{\Psi}_3+\text{H.c.}$$

Hereafter $\Omega_p(\mathbf{r},t)=\mathbf{e}_p\cdot\mathbf{p}_{21}\mathcal{E}_p/\hbar$ and $\Omega_c(\mathbf{r},t)=\mathbf{e}_c\cdot\mathbf{p}_{23}\mathcal{E}_c/\hbar$ are the half Rabi frequencies of the probe and control fields, respectively, $\mathbf{p}_{jj'}$ is the electric dipole matrix element associated with the transition between $|j\rangle$ and $|j'\rangle$, and H.c. stands for the Hermitian conjugate.

Excluding the case of ultralow temperatures at which a Bose-Einstein condensation of atoms can occur, we neglect the two-body interactions. Then, for typical experimental settings one can also safely neglect atomic kinetic energy which is several orders of magnitude less than the internal energy (see also the discussion in Sec. II, below), what corresponds to the approximation $H_i\approx\hbar\omega_i$ $(i=1,2,3)$. Therefore it is convenient to eliminate rapidly the oscillating exponents by means of the transformation $\hat{\Psi}_j(\mathbf{r},t)=\hat{\psi}_j(\mathbf{r},t)\exp(i\{\mathbf{k}_j\cdot\mathbf{r}-[\omega_j-(-1)^j\Delta_j]t\})$, where $\Delta_1=0$, $\Delta_2=(\omega_2-\omega_1)-\omega_p$, and $\Delta_3=\omega_p-\omega_c-(\omega_3-\omega_1)$ are the one- and two-photon detuning (see Fig. 1), and the wave vectors are given by $\mathbf{k}_1=0$, $\mathbf{k}_2=\mathbf{k}_p-\mathbf{k}_c$, and $\mathbf{k}_3=\mathbf{k}_p$.

Next, we recall that due to spontaneous emission there exists a decay of each of the atomic states. The present consideration will be restricted to the situation when the decay rate of the state $|3\rangle$ is very small and can be neglected, which can be realized by choosing $|3\rangle$ as a hyperfine ground state or a metastable state. In order to establish the respective conditions we focus on the more significant losses of the excited states $|2\rangle$, which we account phenomenologically by adding the decay rate $i\gamma_2$ in the Heisenberg equation for $\hat{\psi}_2$:

$$i\frac{\partial\hat{\psi}_1}{\partial t}=-\Omega_p^*\hat{\psi}_2, \tag{2a}$$

$$i\frac{\partial\hat{\psi}_2}{\partial t}=(\Delta_2-i\gamma_2)\hat{\psi}_2-\Omega_p\hat{\psi}_1-2\Omega_c\cos(\mathbf{K}\cdot\mathbf{r})\hat{\psi}_3, \tag{2b}$$

$$i\frac{\partial\hat{\psi}_3}{\partial t}=-\Delta_3\hat{\psi}_3-2\Omega_c^*\cos(\mathbf{K}\cdot\mathbf{r})\hat{\psi}_2. \tag{2c}$$

One can evidently neglect losses associated with the excited state if the atomic system is in the stationary dark state (where the excited state is not populated). Strictly speaking, this is not the case we are dealing with because the dark state is achievable only for the zero two-photon detuning (as this is confirmed below). Nevertheless one can require the system to be in some sense "close" to the dark state where the lost of particles is suppressed. In order to establish these conditions we look for the solution of Eq. (2) in the form $\hat{\psi}_j(\mathbf{r},t)=e^{i\lambda t}\hat{\phi}_j(\mathbf{r})$, where the exponent λ is a slowly varying function of space. This immediately yields the characteristic equation,

$$\lambda^3 - (-\Delta_2 + \Delta_3 + i\gamma_2)\lambda^2 + [\Delta_3(-\Delta_2 + i\gamma_2) - 4|\Omega_c|^2\cos^2(\mathbf{K}\cdot\mathbf{r}) - |\Omega_p|^2]\lambda + |\Omega_p|^2\Delta_3 = 0. \quad (3)$$

Thus, if the two-photon detuning Δ_3 is zero we obtain one of the characteristic values $\lambda=0$, which corresponds to the exact dark state [10] ($n_j=\langle\hat{\phi}_j^\dagger\hat{\phi}_j\rangle$): $n_1=|\Omega_p|^2/[|\Omega_p|^2+4|\Omega_c|^2\cos^2(\mathbf{K}\cdot\mathbf{r})]$ $n_2=0$, and $n_3=4|\Omega_c|^2\cos^2(\mathbf{K}\cdot\mathbf{r})/[|\Omega_p|^2+4|\Omega_c|^2\cos^2(\mathbf{K}\cdot\mathbf{r})]$. In this case, the mean population n_2 of the excited state $|2\rangle$ is zero, and hence the probe beam is exempted from absorption by the atomic medium: it propagates freely and does not display nonlinear effects.

Thus, for the dissipation effects to be negligible and for the nonlinearity to be appreciable, one has to consider the system in a state close to the dark state, which can be achieved for using a small but nonzero Δ_3. In this situation, the population in the excited state $|2\rangle$ is nonzero but small enough in comparison with the total atomic number,

$$\mathcal{N} = n_1 + n_2 + n_3. \quad (4)$$

Then one of the characteristic values of λ can be made very small. Indeed assuming λ small enough we obtain from Eq. (3)

$$\lambda = \frac{|\Omega_p|^2\Delta_3}{\Delta_3(\Delta_2 - i\gamma_2) + 4|\Omega_c|^2\cos^2(\mathbf{K}\cdot\mathbf{r}) + |\Omega_p|^2}. \quad (5)$$

Notice that $\lambda=0$ is achievable only for $\Delta_3=0$, i.e., for the dark state.

Now we define one of our main approximations as

$$\gamma_2 \ll |\Delta_2|. \quad (6)$$

It allows us to consider λ to be real, i.e.,

$$\lambda \approx \lambda_r = \frac{|\Omega_p|^2\Delta_3}{\Delta_2\Delta_3 + 4|\Omega_c|^2\cos^2(\mathbf{K}\cdot\mathbf{r}) + |\Omega_p|^2}. \quad (7)$$

Then the exponent for decay rate of the total number of atoms is estimated as

$$\mathrm{Im}\,\lambda \approx \frac{\Delta_3\gamma_2}{\Delta_2\Delta_3 + 4|\Omega_c|^2\cos^2(\mathbf{K}\cdot\mathbf{r}) + |\Omega_p|^2}\lambda_r, \quad (8)$$

where we have neglected the terms of the γ_2^2 order. Our consideration in what follows is restricted to the nonresonant case, i.e., when the denominator in Eq. (8) is different from zero [see Eq. (16) below]. In such a case weakness of the dissipative losses is determined not only by smallness of γ_2 but also by the low population of the excited state, i.e., by the smallness of Δ_3.

The condition of the smallness of λ is considered in more details in Sec. II B.

B. Polarization

Now we turn to the consideration of the electric field, which is governed by the wave equation,

$$\nabla^2\mathbf{E} - \frac{1}{c^2}\frac{\partial^2\mathbf{E}}{\partial t^2} = \frac{1}{\epsilon_0 c^2}\frac{\partial^2\mathbf{P}}{\partial t^2}, \quad (9)$$

where $\mathbf{P}$ is the polarization induced by the applied electric field $\mathbf{E}=\mathbf{E}_p+\mathbf{E}_c$ given by the expectation value of the atomic dipole moments $\mathbf{p}_{ij}$,

$$\mathbf{P} = \langle\hat{\Psi}_1^\dagger\mathbf{p}_{12}\hat{\Psi}_2\rangle + \langle\hat{\Psi}_3^\dagger\mathbf{p}_{32}\hat{\Psi}_2\rangle + \text{c.c.}$$
$$= \langle\hat{\psi}_1^\dagger\hat{\psi}_2\rangle\mathbf{p}_{12}e^{i(\mathbf{k}_p\cdot\mathbf{r}-\omega_p t)} + \langle\hat{\psi}_3^\dagger\hat{\psi}_2\rangle\mathbf{p}_{32}e^{i(\mathbf{k}_c\cdot\mathbf{r}-\omega_c t)} + \text{c.c.}$$

We will focus on the dynamics of the probe field, which is weak in comparison with the control field,

$$|\Omega| \ll 1, \quad \text{where} \quad \Omega = \frac{\Omega_p}{\Omega_c}. \quad (10)$$

Substituting the expressions for $\mathbf{E}_p$ and $\mathbf{E}_c$ into Eq. (9), we obtain the evolution equation for Ω_p,

$$\left(\nabla^2 - \frac{1}{c^2}\frac{\partial^2}{\partial t^2}\right)\Omega_p e^{i(\mathbf{k}_p\cdot\mathbf{r}-\omega_p t)} = \frac{\mathcal{N}|\mathbf{p}_{12}|^2}{\hbar\epsilon_0 c^2}\frac{\partial^2}{\partial t^2}\langle\hat{\psi}_1^\dagger\hat{\psi}_2\rangle e^{i(\mathbf{k}_p\cdot\mathbf{r}-\omega_p t)}. \quad (11)$$

By using Eq. (2) with $\lambda=\lambda_r$, given by Eq. (7), and conservation of particle number [Eq. (4)], we obtain

$$\langle\hat{\psi}_1^\dagger\hat{\psi}_2\rangle = \frac{\Lambda(\delta_3-\Lambda)^2\Omega}{(\Lambda^2+|\Omega|^2)(\delta_3-\Lambda)^2 + 4\Lambda^2\cos^2(\mathbf{K}\cdot\mathbf{r})}, \quad (12)$$

where we have introduced the dimensionless parameters [see Eq. (7)],

$$\Lambda = \frac{\lambda_r}{|\Omega_c|} = \frac{\delta_3|\Omega|^2}{|\Omega|^2 + \delta_2\delta_3 + 4\cos^2(\mathbf{K}\cdot\mathbf{r})} \quad (13)$$

and $\delta_j=\Delta_j/|\Omega_c|$.

Notice that there is an important conclusion following from Eqs. (2a) and (4): the condition for the excited state $|2\rangle$ to be weakly populated, i.e., to have $n_2\ll\mathcal{N}$, is equivalent to the requirement $|\lambda_r|\ll|\Omega_p|$, which is the same as

$$\Lambda \ll 1. \quad (14)$$

Further simplification can be achieved if one of the conditions,

$$\delta_2\delta_3 > 0 \quad \text{or} \quad \delta_2\delta_3 < -4, \quad (15)$$

is fulfilled. Then one has that for all values of $\mathbf{K}\cdot\mathbf{r}$,

$$v(\mathbf{K}\cdot\mathbf{r}) \equiv \delta_2\delta_3 + 4\cos^2(\mathbf{K}\cdot\mathbf{r}) \neq 0. \quad (16)$$

From Eqs. (12) and (13) we see that in this situation $\langle\hat{\psi}_1^\dagger\hat{\psi}_2\rangle$ is always bounded. Indeed, since now $|\Lambda|\neq|\delta_3|$, we have the following estimate:

$$|\langle\hat{\psi}_1^\dagger\hat{\psi}_2\rangle| \leq \frac{|\Lambda\Omega|}{\Lambda^2+|\Omega|^2} \leq \frac{1}{2}. \quad (17)$$

Finally, using expression (13) under assumption (10) one can approximate Eq. (12) as

$$\langle \hat{\psi}_1^\dagger \hat{\psi}_2 \rangle = \frac{\delta_3 \Omega}{v(\mathbf{K}\cdot\mathbf{r})}\left[1 - \frac{\delta_3^2 - \delta_2\delta_3 - 2v(\mathbf{K}\cdot\mathbf{r})}{v^2(\mathbf{K}\cdot\mathbf{r})}|\Omega|^2\right], \tag{18}$$

where we have neglected the Ω^5-order terms.

III. SPATIAL OPTICAL SOLITONS AND INSTABILITIES OF THE PROBE BEAM

A. Envelope equation for Ω

Let us now consider several interesting situations addressing the geometry of the control field, which creates different optical lattices for the probe field. To be specific, we limit ourselves to a one-dimensional (1D) lattice that has different spatial orientations. For simplicity, we focus on the following two cases:

(i) *Case A*: $\mathbf{K}=K\mathbf{e}_x$ (the upper inset in Fig. 1);

(ii) *Case B*: $\mathbf{K}=K\mathbf{e}_z$ (the lower inset in Fig. 1).

We are interested in spatial patterns resulting from the interplay between the diffraction and nonlinearity when the probe field passes through the atomic cloud. Therefore we require Ω to be independent on time. Substituting Eq. (18) into the wave [Eq. (11)] and using slowly varying envelope approximation, we obtain the dimensionless nonlinear Schrödinger (NLS) equation for Ω with linear and nonlinear coefficients being periodic functions of the spatial coordinates:

$$2i\frac{\partial\Omega}{\partial\zeta} + \frac{\partial^2\Omega}{\partial\xi^2} + \frac{\partial^2\Omega}{\partial\eta^2} + \frac{\wp\Omega}{v(\vec{\kappa}\cdot\vec{\rho})} - \wp g(\vec{\kappa}\cdot\vec{\rho})|\Omega|^2\Omega = 0. \tag{19}$$

Here $v(\vec{\kappa}\cdot\vec{\rho}) \equiv v(\mathbf{K}\cdot\mathbf{r})$ is given by Eq. (16),

$$g(\vec{\kappa}\cdot\vec{\rho}) = \frac{\delta_3^2 - \delta_2\delta_3 - 2v(\vec{\kappa}\cdot\vec{\rho})}{v^3(\vec{\kappa}\cdot\vec{\rho})}, \quad \wp = \frac{\mathcal{N}|\mathbf{p}_{12}|^2}{\hbar\epsilon_0\Omega_c^2}\Delta_3,$$

and we have introduced the dimensionless variables $k_p\mathbf{r}=\vec{\rho}=(\xi,\eta,\zeta)$ and $\vec{\kappa}=\mathbf{K}/k_p$.

First of all we notice that in all the cases considered below there exists the limit of a constant coupling field which can be formally obtained by putting $\mathbf{K}=0$. In this limit $v(\cdot)$ and $g(\cdot)$ become constants, and Eq. (20) is the well known (2+1)-*D* NLS equation which supports only unstable Townes solitons for $\varsigma=-1$ and has no stationary spatially localized solutions for $\varsigma=1$. In other words no stable localized light channels can be created in the atomic cloud in that case.

In Secs. III B and III C we show that OL can completely change the situation and subject to properly chosen parameters can stabilize light channels. We analyze different dynamical regimes described by the model [Eq. (19)] for $\mathbf{K}\neq 0$ and provide their numerical simulations. To this end we have to specify numerical values for the main physical parameters, which are feasible experimentally. The system we are dealing with is a laser-cooled gas of magnesium atoms, whose parameters can be found, say, in Ref. [12]. In this system the atomic states $|1\rangle$, $|2\rangle$, and $|3\rangle$ can be chosen as $^3S_0$, $^3P_1$, and $^3P_0$, respectively. The wavelengths of the probe and control beams are chosen as $\lambda_p=2\pi/k_p=457$ nm and $\lambda_c=2\pi/k_c=0.5$ mm, respectively. One of the advantages of the chosen system is that atoms possess long decay time even for their excited states. The decay time of $|2\rangle$ is about 5.1 ms. Hence, the condition $\gamma_2 \ll |\Delta_2|$ used in Eq. (6) can be easily fulfilled provided that the one-photon detuning Δ_2 is chosen of order of 10^7 s^{-1}. In all numerical simulations given below, the atomic concentration $\mathcal{N}$ is taken as 1.0×10^{14} cm^{-3}. For the convenience of the following classification, we define the direction of $\mathbf{K}$ as that of the optical lattice.

B. Diffraction parallel to the optical lattice: Spatial solitons

We first consider case A, for which the diffraction (characterized by the dependence on the coordinated ξ and η) is parallel to the optical lattice. Since $\vec{\kappa}=\kappa\mathbf{e}_x$, Eq. (19) reads as

$$2i\frac{\partial\mathcal{A}}{\partial\zeta} + \frac{\partial^2\mathcal{A}}{\partial\xi^2} + \frac{\partial^2\mathcal{A}}{\partial\eta^2} + \frac{\wp}{v(\kappa\xi)}\mathcal{A} - \varsigma g(\kappa\xi)|\mathcal{A}|^2\mathcal{A} = 0, \tag{20}$$

where $\mathcal{A}=\sqrt{|\wp|}\Omega$ and $\varsigma=\mathrm{sgn}(\Delta_3)$.

If there is no modulation of the nonlinearity, i.e., $g(\kappa\xi)$ is a constant, but the linear lattice is held; Eq. (20) can support 2D solitons, stabilized by the 1D optical lattice [11] provided the nonlinearity is focusing. With an additional modulation in the nonlinearity, we anticipate that Eq. (20) still supports stable (not necessarily stationary, however) localized structures at least for negative $\varsigma g(\kappa\xi)$ in the whole space. This last condition can be satisfied for $\delta_3>0$ combined with either for $\delta_3^2<3\delta_2\delta_3$ or for $\delta_2\delta_3<-4$ [see also Eq. (15)].

In order to check this, we have performed numerical simulations of Eq. (20) by employing a pseudospectral method combined with a second-order split-step method to advance in the "time" coordinate ζ. We choose $\Delta_2=1.4\times10^7$ s^{-1}, $\Delta_3=1.0\times10^6$ s^{-1}, and $\Omega_c=2.4\times10^6$ s^{-1}. Notice that with these parameter values we have $\delta_3^2<3\delta_2\delta_3$ and $\varsigma=1$.

Typical results of the numerics are shown in Fig. 2. Shown in the bottom-right panel is the maximal intensity of $|\mathcal{A}|^2$ as a function of ζ. From the figure we observed that strong diffraction of the Gaussian input beam is indeed prevented by the linear lattice in Eq. (20). The evolution however has an oscillatory character due to the nonlinear lattice effect. The intensity (radius) of the beam periodically decreases (increases) as ζ grows. The period (denoted by $\mathcal{Z}$) for the reappearance of the principal maxima is approximately $\mathcal{Z}=80$. We also observe shallow stripes appearing due to the periodical modulation of the medium properties along the x axis.

We have repeated simulations with different amplitudes of the input beam A_0 and different lattice constants d. The results show that $\mathcal{Z}$ increases slightly with A_0 and d. We also found a threshold amplitude (i.e., the amplitude below which no solitons are created) for the Gaussian beam with $d=\pi/10$ is approximately $A_{th}=0.07$. For such a beam the maximum input intensity can be estimated by the formula $I_{\max}=c\epsilon_0|\mathbf{E}_{p\,\max}|^2/2$. Using the above parameters we obtain

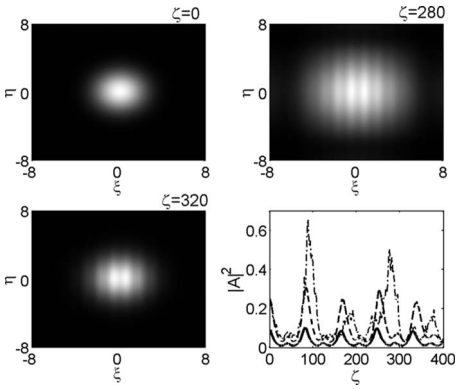

FIG. 2. Snapshots of the intensity $|\mathcal{A}|^2$ for different instants ζ and the initial $\mathcal{A}_0=A_0\exp[-(\xi^2+\eta^2)/9.0]$, with $A_0=0.3$ and the lattice constant $d=\pi/10$. The brightness is proportional to the magnitude of intensity. The left panels correspond to principal maxima and the upper-right panel to a local minimum of the evolution of the maximal intensity shown in the bottom-right panel by the solid line. In the latter the dashed and dash-dotted lines correspond to the initial condition with $A_0=0.5$ and the lattice constants $d=\pi/10$ and $\pi/5$.

$I_{\max}\approx 0.13\times 10^{-7}$ W cm^{-2}. Thus, to produce a (2+1)-*D* spatial optical soliton similar to one shown in Fig. 2, a very low input light intensity is needed. We remark that the intensity of a single 500 nm photon per nanosecond on an area of 1 μm^2 is $I_{ph}=0.04$ W cm^{-2}. This shows that our scheme makes it possible to generate a 2D spatial soliton with a single-photon wave packet. This is in a sharp contrast with the case of nonresonant media, where very high input intensities or very long optical paths are necessary to originate nonlinear effect required for soliton formation, and even with the earlier EIT schemes whether either quintic [6] or saturable [7] nonlinearities were necessary. The optical lattice now plays the role of the stabilizing factor.

C. Diffraction parallel to the optical lattice: Instabilities

1. Envelope equation

Next, we consider the situation where the characteristic transverse size of the probe beam is much larger than the lattice period *d*. Assuming smallness of the nonlinearity, i.e., of the intensity of the field [Eq. (10)], we employ the multiple-scale expansion to simplify Eq. (19). To this end we introduce normalized Bloch functions $u_{m,k}(\xi)$ $[(\int_0^{2d}|u_{m,k}(\xi)|^2d\xi=1)]$,

$$\hat{\mathcal{L}}u_{m,k}(\xi)=-q_{m,k}^2u_{m,k}(\xi),\quad \hat{\mathcal{L}}=-\frac{\partial^2}{\partial\xi^2}-\frac{\wp}{v(\xi)},\qquad (21)$$

where the indices *m* and *k* stand for the band number and the wave vector in the first Brillouin zone, i.e., for $k\in[-\kappa,\kappa]$, respectively.

The dependence of the wave vector *q* (i.e., of the *y* projection) on the *x*-projection *k* determines the deviation of the angle of incidence of the probe beam from the *z* axis. It has a band structure, two examples of which are illustrated in Fig. 3, where the lowest bands with $m=1$ and $m=1,2$ are shown.

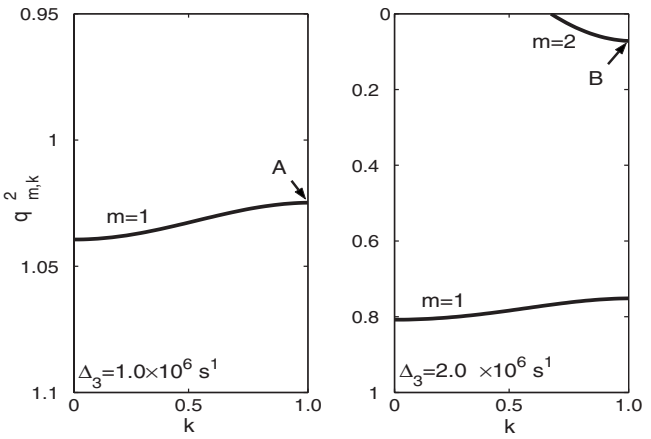

FIG. 3. Two examples of the band structures for $-q_{m,k}^2$ for the optical lattice with the period $d=\pi$.

Below we concentrate on the particular where $k=\kappa$, and $q_{m,k}$ borders a gap edge (examples are indicated by the points A and B in Fig. 3). For the sake of convenience we introduce simplified notations $q_m=q_{m,\kappa}$ and $u_m(\xi)=u_{m,\kappa}(\xi)$ and define the diffraction coefficient $\mathcal{D}$ and the effective nonlinearity $\mathcal{G}$ given, respectively, by

$$\mathcal{D}=\frac{1}{2}\frac{d^2q_m}{dk^2}\quad\text{and}\quad\mathcal{G}=\int_0^{2d}g(\kappa\xi)|u_m(\xi)|^4d\xi.$$

Now the probe beam field is searched in the form $\Omega=\sqrt{2/|\wp\mathcal{G}|}\mathcal{A}(\xi,\eta',\zeta)u_m(\xi)$, where the slowly varying amplitude $\mathcal{A}$ is governed by the NLS equation,

$$2i\frac{\partial\mathcal{A}}{\partial\zeta}+\mathcal{D}\frac{\partial^2\mathcal{A}}{\partial\xi^2}+\frac{\partial^2\mathcal{A}}{\partial\eta'^2}-2\sigma|\mathcal{A}|^2\mathcal{A}=0,\qquad (22)$$

with $\eta'=(1+q_m^2)^{-1/2}(\eta-q_m\zeta)$ and $\sigma=\mathrm{sgn}(\Delta_3\mathcal{G})$, which is obtained by means of the multiple-scale expansion (outlined in Appendix A).

In the case at hand both $\mathcal{D}$ and $\Delta_3\mathcal{G}$ can be either positive or negative. Hence Eq. (22) can describe by any one of the following cases:

(1) Elliptic diffraction and self-focusing nonlinearity ($\mathcal{D}>0$ and $\sigma=-1$);

(2) Elliptic diffraction and self-defocusing nonlinearity ($\mathcal{D}>0$ and $\sigma=1$);

(3) Hyperbolic diffraction and self-focusing nonlinearity ($\mathcal{D}<0$ and $\sigma=-1$);

(4) Hyperbolic diffraction and self-defocusing nonlinearity ($\mathcal{D}<0$ and $\sigma=1$).

2. Instabilities of solitons of Eq. (22): Elliptic cases

The elliptic case where $\mathcal{D}>0$ has been extensively studied in literature (see e.g., [13,14]), and therefore we give only a brief summary of the results relevant to the present work. When the nonlinearity is self-focusing ($\sigma=-1$) a planar bright soliton solution of Eq. (22) reads as

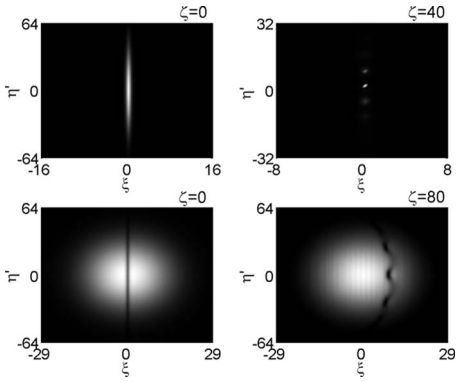

FIG. 4. Snapshots of the intensity $|\mathcal{A}_b|^2$ for different ζ for a bright input soliton [Eq. (22)] with the initial conditions, $\mathcal{A}_b(\xi,\eta',\zeta=0)=0.8\ \mathrm{sech}(0.8\xi)[1.0+0.01\ \exp(i\eta)]\exp[-(\xi^2+\eta'^2)/1600]$ (the upper panels), and for a dark soliton, $\mathcal{A}_d(\xi,\eta',\zeta=0)=[0.8\ \tanh(0.8\xi)+i0.6]\exp[-(\xi^2+\eta'^2)/1600]+0.1\{0.64[1-\tanh\times(0.8x)^2]\}\cos(0.1y)$, corresponding to $\theta=0.88$ in Eq. (24) (the lower panels). The brightness denotes the magnitude of intensity.

$$\mathcal{A}_b(\xi,\zeta)=\frac{1}{\ell}\,\mathrm{sech}\left(\frac{\xi-\nu\zeta}{\ell}\right)e^{i[\nu\xi-(\nu^2-1/\ell)\zeta/2]}. \tag{23}$$

Here $2\nu=\tan\theta$, where θ is the angle between the soliton axis and z axis, and ℓ is the width of the beam in the x direction. This solution is however unstable [15] with respect to transverse perturbations $\sim e^{ip\eta}$ having wave numbers within the interval $p^2<3/\ell$ [16]. The instability leads to filamentation of the beam at a finite propagating distance (see the upper panels of Fig. 4).

When nonlinearity is defocusing ($\sigma=1$), the carrier wave solution is stable and supports a dark soliton,

$$\mathcal{A}_d(\xi,\zeta)=\left[\frac{1}{\ell}\tanh\left(\frac{\xi-\nu\zeta}{\ell}\right)+i\nu\right]e^{-i\rho^2\zeta}, \tag{24}$$

where ρ is the amplitude of the background, ℓ is the width of the soliton and $\nu=\tan\theta=\sqrt{\rho^2-\ell^{-2}}$. The solution [Eq. (24)] is also unstable with respect to transverse perturbations [17]: in the course of evolution the soliton decays into a train of vortices with alternative polarities [18] (see the lower panels of Fig. 4).

The optical lattice allows one to control which of the instabilities is developed. Indeed, let us consider the band structure shown in Fig. 3. By fixing the wave vector to border the boundary of the Brillouin zone ($k=\kappa$), one obtains a set of available values q_m^2 (as the ones shown by the points A and B). Taking also into account that the wavelength λ_p is fixed, by the given one- and two-photon detunings one obtains that the direction of the propagation of the probe beam, and hence the σ is also uniquely fixed and can be changed by changing the angle of incidence. For each of the directions, one can compute the respective diffraction coefficient (say, in point A one obtains $q_m=1.0$ and $\mathcal{D}\approx 0.1$ for $\Delta_3=1.0\times 10^6\ \mathrm{s}^{-1}$).

In order to illustrate the spatial evolution of the beam intensities corresponding to bright [Eq. (23)] and dark [Eq. (24)] soliton distributions, accounting also the finite size of the beam in y direction (as this happens in real experiments), we performed numerical simulations of Eq. (22) subject to the respective initial conditions with small initial perturbations. The parameters were taken the same as those used in Sec. III B for bright solitons, except for two-photon detuning which is now $\Delta_3=-2.0\times 10^6\ \mathrm{s}^{-1}$ (respectively, $\delta_2\delta_3=-4.9<-4$).

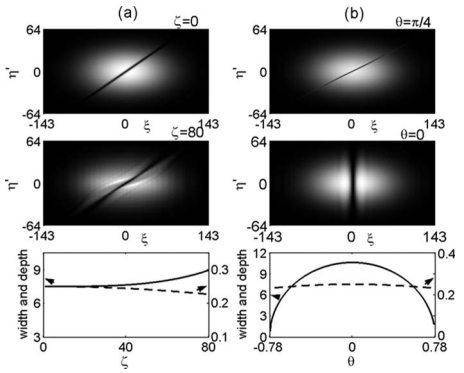

FIG. 5. (a) Snapshots of the intensity $|\mathcal{A}|^2$ different $\zeta=0$ (the top panel) and $\zeta=80$ (the middle panel). The initial condition is given by $\mathcal{A}_0=0.5\ \tanh[0.7(\xi-0.7\eta')]\exp[-(\xi^2+\eta'^2)/1600]$ (the Gaussian background is added to simulate more realistic experimental situations). The bottom panel shows the width (solid line) and depth (dashed line) of the soliton vs ζ. (b) (Right column) The snapshots of the intensity at $\zeta=40$ for different θ. The bottom panel illustrates the dependence of the width (solid line) and the depth (dashed line) on θ.

The results are shown in Fig. 4. In the simulations, conservation laws for the intensity and energy of the probe beam were monitored. The results were also tested on different grid sizes and time steps. From the right top panel one observes filamentation instability. The maximum intensity of the created narrow beams increases for approximately three times during the simulation. In the lower panels of Fig. 4 one can see the breaking down of the dark soliton and its decay into a set of vortices. Finally, we notice that the observation of bright and dark soliton phenomena, and their instabilities predicted above requires atomic clouds with the transverse and longitudinal dimensions of order of 10^{-3} and 10^{-4} cm.

3. Instabilities of solitons of Eq. (22): Hyperbolic cases

The hyperbolic diffraction ($\mathcal{D}<0$) is less studied in the literature [14]. Now, as an ansatz for a stationary solution of Eq. (22) we take $\mathcal{A}(\xi,\eta',\zeta)=\mathcal{F}(\xi,\eta')\exp(2i\beta\zeta)$, where β is the propagation constant and $\mathcal{F}(\xi,\eta')$ reads (a dark soliton solution) as

$$\mathcal{F}=\rho\,\tanh\left[\frac{1}{\ell}(\xi-2\nu\eta')\right],\quad \ell^2=\frac{|\mathcal{D}|-\tanh^2\theta}{\rho^2} \tag{25}$$

(here the rotation angle in the (x,y) plane is defined by $\tan\theta=2\nu$, see Fig. 5). For such a solution the angle θ is limited by the dispersion coefficient and thus by the depth of the optical lattice: in a general situation shallow lattices allow for wider range of the rotation angles.

The conditions for the hyperbolic diffraction can be created by adjusting the geometry of the incident beam. For

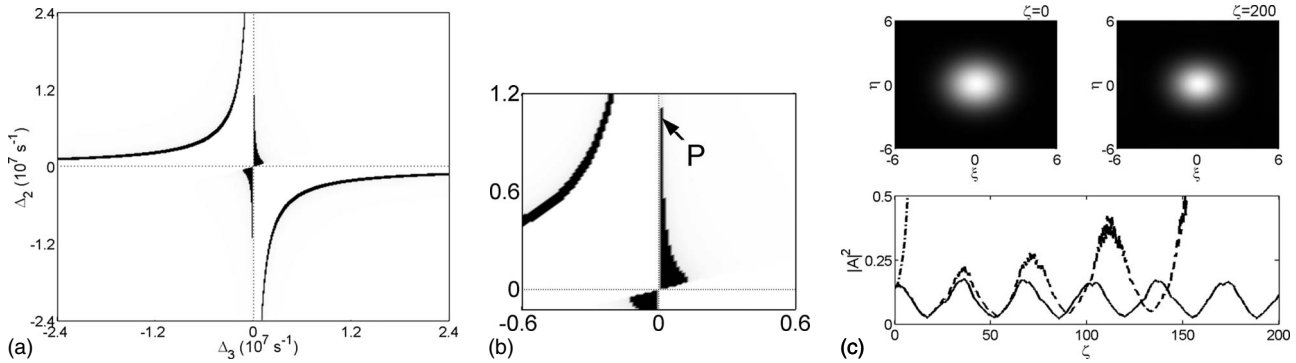

FIG. 6. (a) Regions of the beam stabilization (shadowed part) vs the photon detunings for the lattice constant $d=\pi/20$. More details are shown in (b). (c) Snapshots of the intensity evolution of the initial Gaussian beam with $W_0=1.5$ at $\Delta_2=1.0\times10^7$ s^{-1} and $\Delta_3=1.0\times10^5$ s^{-1} (the point P in the top panel, notice now $\delta_2\delta_3=0.17>0$). The other parameters are the same as in Sec. II B. (c, lower panel) The maximum $|\mathcal{A}|^2$ vs ζ of the Gaussian beam. The solid, dashed, and dot-dashed lines denote, respectively, the cases with fast ($d=\pi/20$), slow ($d=\pi/3$), and no modulation of the nonlinearity.

example, taking $\Delta_2=2.0\times10^7$ s^{-1} and other parameters as in Sec. III B, we obtain $q_m=0.3$ (corresponding to the point B in the right panel of Fig. 3) and $\mathcal{D}=-5.0$. These data can be used to test the stability of solution (25) by solving numerically Eq. (22) subject to initial condition (25). The results are shown in Fig. 5. From the bottom panel we observe that the pattern is relatively robust for $\zeta<40$ and undergoes an apparent deformation for larger ζ. The instability arises from the background: it is likely to be destroyed by growing perturbations, which limits possibilities of observation of a dark soliton.

From Eq. (25) it follows that the width of the soliton changes when its axis rotates. This asymmetric effect is illustrated in Fig. 5 (the right column). We observe that the width goes to zero when $\theta\to\pm\pi/4$ and achieves its maximum when $\theta=0$ (the depth is not sensitive to the rotation).

D. Diffraction orthogonal to the optical lattice

Finally, we analyze Eq. (19) for the situation of the light propagation in the direction parallel to the optical lattice (the case B in the inset of Fig. 1). Then Eq. (19), after the phase renormalization $\mathcal{A}=\sqrt{|\wp|}\Omega\exp[-\frac{i}{2}\int_0^\zeta d\zeta/v(\kappa\zeta)]$, reads as

$$2i\frac{\partial\mathcal{A}}{\partial\zeta}+\frac{\partial^2\mathcal{A}}{\partial\xi^2}+\frac{\partial^2\mathcal{A}}{\partial\eta^2}-\varsigma g(\kappa\zeta)|\mathcal{A}|^2\mathcal{A}=0. \tag{26}$$

This equation displays several interesting effects, among which we mention stabilization of 2D optical solitons [19] and 2D matter wave solitons [20,21], as well as enhancement of collapse at a finite time [22]. In the case at hand either of the above phenomena can be achieved simply by changing the parameters of the optical lattice or of the photon detunings.

Concentrating on stabilization of a beam, we notice that it admits rather complete analytical description in terms of the momentum method [20]. In particular, the necessary condition for stabilizing 2D solitons of Eq. (26) consists of the inequality,

$$Q_1 d+Q_2\int_0^d g(\kappa\zeta)d\zeta<0, \tag{27}$$

and the requirement for the quantity $Q_1+Q_2g(\kappa\zeta)$ to change the sign. The definition of Q_1 and Q_2, as well the derivation of Eq. (27) are given in Appendix B.

As an example we consider an input Gaussian pulse $\mathcal{A}(\xi,\eta,\zeta=0)=\exp[-(\xi^2+\eta^2)/(2W_0^2)]/(\sqrt{\pi}W_0)$ (W_0 is a constant) for which $Q_1=1/(2\pi)^2$ and $Q_2=1/(2\pi)^3$. Then the region of the beam stabilization by the lattice with $d=\pi/20$ is shown in Fig. 6. In the same figure we also show the typical result of the evolution of the stabilized soliton. One indeed observes in Fig. 6 that for a small enough lattice constant d the probe beam focusing is inhibited. Increasing d leads to the beam focusing at a finite distance, which is however larger than its counterpart in the continuous medium, where self-focusing of the same input beam occurs at very early stage of the evolution (see the bottom panel). In other words one can advance or delay, i.e., to manage, focusing by changing the angle between two copropagating control fields creating optical lattice [this affects the period of spatial modulation appearing in the nonlinear coefficient of Eq. (26)].

The maximum input intensity in Fig. 6, estimated as $I_{\max}=c\epsilon_0|\mathbf{E}_{p,\max}|^2/2$, for the parameters described above gives $I_{\max}\approx0.6\times10^{-5}$ W cm^{-2}. We thus again arrive at the conclusion that the lattice allows for producing a high-dimension spatial optical soliton with an intensity of a single-photon wave packet.

IV. CONCLUSION

In the present paper we have shown that resonant optical lattice formed by a control field in an atomic Λ system can create conditions for propagation of a weak probe field such as a tunable band-gap structure in the regime of electromagnetically induced transparency. Such a system possesses many striking properties, among which we mention the decrease in probe-beam absorption, enhancement of Kerr nonlinearity, on the one hand, and stabilizing effect, allowing for generation spatial solitons at extremely low intensities, on

the other hand. In addition, this system has the advantage that it is easy to be implemented and manipulated in experiments, and hence it may serve as a nice test bed for various linear and nonlinear phenomena that has been investigated in conventional periodic materials by using very low light intensity. Also the proposed scheme allows one to generate various scenarios of instabilities and self-focusing.

A remarkable property is that change from one scenario of the beam evolution to another can be achieved simply by "geometrical" means, i.e., by changing angles of either coupling or probe beams. Naturally, all the mentioned phenomena were described within the framework of a unified theory and were illustrated by direct numerical simulations. The results we obtained may have potential applications in optical information processing and engineering.

ACKNOWLEDGMENTS

C.H. was supported by the FCT under Grant No. SFRH/BPD/36385/2007. G.H was supported by the NSFC under Grant Nos. 10674060 and 10874043 and by the Key Development Program for Basic Research of China under Grant Nos. 2005CB724508 and 2006CB921104.

APPENDIX A: DERIVATION OF EQ. (22)

We use the multiple-scale expansion, which is a standard technique for the cases where the lattice constant is much less than the characteristic scale of the field pattern (see e.g., [23]). To this end we introduce a formal small parameter $\epsilon \ll 1$ (which at the end of calculations must be made one) and independent variables $(\xi_l, \eta_l, \zeta_l) = \epsilon^l(\xi, \eta, \zeta)$. We look for the field in the form $\Omega = e^{iq\eta_0} \Sigma_{j=1}^{\infty} \epsilon^j \Omega^{(j)}(\xi_0, \xi_1, \eta_1, \zeta_2)$, where $\Omega^{(j)} = O(1)$, are functions of the scaled variables among which we indicate in the arguments only the most rapid ones, i.e., $\Omega^{(j)}(\xi_0, \eta_1, \zeta_1) \equiv \Omega^{(j)}(\xi_0, \xi_1, \ldots, \eta_1, \eta_2, \ldots, \zeta_1, \zeta_2, \ldots)$. Substituting this expansion in Eq. (19) and collecting the terms at each order of ϵ, we obtain

$$\hat{\mathcal{L}}\Omega^{(j)} + q^2\Omega^{(j)} = F_j, \quad j = 1,2, \ldots , \tag{A1}$$

where $\hat{\mathcal{L}}$ is defined in Eq. (21), $F_1 = 0$,

$$F_2 = 2i\frac{\partial \Omega^{(1)}}{\partial \zeta_1} + 2\frac{\partial^2 \Omega^{(1)}}{\partial \xi_0 \partial \xi_1} + 2iq\frac{\partial \Omega^{(1)}}{\partial \eta_1},$$

$$F_3 = 2i\frac{\partial \Omega^{(1)}}{\partial \zeta_2} + \frac{\partial^2 \Omega^{(1)}}{\partial \xi_1^2} + \frac{\partial^2 \Omega^{(1)}}{\partial \eta_1^2} + \frac{\partial^2 \Omega^{(1)}}{\partial \zeta_1^2} + 2i\frac{\partial \Omega^{(2)}}{\partial \zeta_1} + 2\frac{\partial^2 \Omega^{(2)}}{\partial \xi_0 \partial \xi_1} + 2iq\frac{\partial \Omega^{(2)}}{\partial \eta_1} - \wp g(\xi_0)|\Omega^{(1)}|^2\Omega^{(1)}.$$

The solution of Eq. (A1) at $j=1$, which corresponds to the wave vector bordering a gap edge κ is searched in the form of $\Omega^{(1)} = A(\xi_1, \eta_1, \zeta_2)u_m(\xi_0)$, where $u_m(\xi_0)$ is a real $2d$-periodic function.

A solution for the second order is searched in the form $\Omega^{(2)} = \Sigma_{n \neq m} B_{nm}(\xi_1, \eta_1, \zeta_2)u_n(\xi_0)$, where the envelope amplitudes B_{nm} are obtained by applying $\int_0^{2d} d\xi_0 u_n(\xi_0)$:

$$B_{nm} = \frac{2}{q_m - q_n}\frac{\partial A}{\partial \xi_1}\int_0^{2d} u_n(\xi)\frac{\partial}{\partial \xi}u_m(\xi)d\xi. \tag{A2}$$

The solvability condition of the second order of Eq. (A1) reads as $(\partial A/\partial \zeta_1) + q_m(\partial A/\partial \eta_1) = 0$. Then, defining $\rho = \eta_1 - q_m\zeta_1$, we can write $A(\xi_1, \eta_1, \zeta_1) \equiv A(\xi_1, \rho)$.

Applying $\int_0^{2d} d\xi_0 \bar{u}_m(\xi_0)$ (an overbar stands for complex conjugation) to the third order of Eq. (A1), we obtain

$$2i\frac{\partial A}{\partial \zeta_2} + \mathcal{D}\frac{\partial^2 A}{\partial \xi_1^2} + (1 + q_m^2)\frac{\partial^2 A}{\partial \rho^2} - \wp\mathcal{G}|A|^2 A = 0, \tag{A3}$$

with $\mathcal{D}$ and $\mathcal{G}$ defined in Eq. (22). Substitution of $A = \sqrt{2/|\wp\mathcal{G}|}\mathcal{A}$ into Eq. (A3) gives Eq. (22).

APPENDIX B: THE CONDITIONS FOR STABILIZING SOLITONS IN EQ. (26)

We follow Ref. [20] to describe radially symmetric 2D localized solutions of Eq. (26). This is done by analyzing integral quantities (here $r^2 = \xi^2 + \eta^2$ and the case $\varsigma = 1$ is considered) as follows:

$$I_1 = \int_0^{\infty} |\mathcal{A}|^2 r dr, \quad I_2 = \int_0^{\infty} |\mathcal{A}|^2 r^3 dr,$$

$$I_3 = i\int_0^{\infty} \left(\mathcal{A}\frac{\partial \bar{\mathcal{A}}}{\partial r} - \bar{\mathcal{A}}\frac{\partial \mathcal{A}}{\partial r}\right) r dr,$$

$$I_4 = \int_0^{\infty} \left(\left|\frac{\partial \mathcal{A}}{\partial r}\right|^2 + g(\zeta)|\mathcal{A}|^2\right) r dr, \quad I_5 = \int_0^{\infty} |\mathcal{A}|^4 r dr.$$

Equations for ζ evolution of $I_j(\zeta)$ $(j = 1, \ldots, 5)$ can be closed subject to the assumption $\arg \mathcal{A} \approx I_3 r^2/(4I_2)$. Then there exist invariants $Q_1 = 2(I_4 - gI_5)I_2 - I_3^2/4$ and $Q_2 = 2I_2 I_5$ allowing to close the equation for $W(\zeta) = \sqrt{I_2(\zeta)}W^3(d^2W/d\zeta^2) = Q_1 + Q_2 g(\zeta)$. From the analysis of the solution of this equation, one obtains the condition of the beam stabilization [20].

[1] G. P. Agrawal, *Nonlinear Fiber Optics* (Academic, New York, 2001); A. Hasegawa and M. Matsumoto, *Optical Solitons in Fibers* (Springer, Berlin, 2003).

[2] S. E. Harris, Phys. Today **50**(7), 36 (1997); M. Fleischhauer, A. Imamoglu, and J. P. Marangos, Rev. Mod. Phys. **77**, 633 (2005).

[3] L. V. Hau, S. E. Harris, Z. Dutton, and C. H. Behrrozi, Nature (London) **397**, 594 (1999); M. M. Kash, V. A. Sautenkov, A. S. Zibrov, L. Hollberg, G. R. Welch, M. D. Lukin, Y. Rostovtsev, E. S. Fry, and M. O. Scully, Phys. Rev. Lett. **82**, 5229

(1999).

[4] H. Schmidt and A. Imamoglu, Opt. Lett. **21**, 1936 (1996); D. Petrosyan and G. Kurizki, Phys. Rev. A **65**, 033833 (2002).

[5] Y. Wu and L. Deng, Phys. Rev. Lett. **93**, 143904 (2004); Opt. Lett. **29**, 2064 (2004); G. Huang, L. Deng, and M. G. Payne, Phys. Rev. E **72**, 016617 (2005); C. Hang, G. Huang, and L. Deng, *ibid.* **73**, 036607 (2006).

[6] H. Michinel, M. J. Paz-Alonso, and V. M. Pérez-García, Phys. Rev. Lett. **96**, 023903 (2006).

[7] C. Hang, G. Huang, and L. Deng, Phys. Rev. E **74**, 046601 (2006).

[8] J. D. Joannopoulos, R. D. Meade, and J. N. Winn, *Photopic Crystals: Molding the Flow of Light* (Princeton University Press, Princeton, NJ, 2001).

[9] M. Bajcsy, A. S. Zibrov, and M. D. Lukin, Nature (London) **426**, 638 (2003); H. Y. Ling, Y. Li, and M. Xiao, Phys. Rev. A **57**, 1338 (1998); Y. V. Rostovtsev, A. B. Matsko, and M. O. Scully, *ibid.* **57**, 4919 (1998); **60**, 712 (1999); A. Andre and M. D. Lukin, Phys. Rev. Lett. **89**, 143602 (2002); F. E. Zimmer, A. Andre, M. D. Lukin, and M. Fleischhauer, Opt. Commun. **264**, 441 (2006); M. Artoni and G. C. La Rocca, Phys. Rev. Lett. **96**, 073905 (2006); K. R. Hansen and K. Mølmer, Phys. Rev. A **75**, 053802 (2007); I. Friedler, G. Kurizki, and D. Petrosyan, *ibid.* **71**, 023803 (2005); D. Petrosyan, *ibid.* **76**, 053823 (2007).

[10] In fact, there are two additional complex characteristic values of λ, which, however, do not give dark state and corresponding $\hat{\psi}_j(\mathbf{r},t)$ decay very rapidly and hence will not be considered here.

[11] B. B. Baizakov, B. A. Malomed, and M. Salerno, Phys. Rev. A **70**, 053613 (2004).

[12] A. Godone and C. Novero, Phys. Rev. A **45**, 1717 (1992).

[13] H. A. Haus and W. S. Wong, Rev. Mod. Phys. **68**, 423 (1996).

[14] Y. S. Kivshar and D. E. Pelinovsky, Phys. Rep. **331**, 117 (2000).

[15] V. E. Zakharov and A. M. Rubenchik, Sov. Phys. JETP **38**, 494 (1974).

[16] L. M. Degtyarev, V. E. Zakharov, and L. I. Rudakov, Sov. Phys. JETP **41**, 57 (1975).

[17] E. A. Kuznetsov and S. K. Turitsyn, Sov. Phys. JETP **67**, 1583 (1988).

[18] C. T. Law and G. A. Swartzlander, Jr., Opt. Lett. **18**, 586 (1993); P. Wolf, Phys. Rev. A **51**, 5016 (1995).

[19] I. Towers and B. A. Malomed, J. Opt. Soc. Am. B **19**, 537 (2002).

[20] G. D. Montesinos, V. M. Pérez-García, and P. Torres, Physica D **191**, 193 (2004).

[21] H. Saito and M. Ueda, Phys. Rev. Lett. **90**, 040403 (2003); F. K. Abdullaev, J. G. Caputo, R. A. Kraenkel, and B. A. Malomed, Phys. Rev. A **67**, 013605 (2003).

[22] V. V. Konotop and P. Pacciani, Phys. Rev. Lett. **94**, 240405 (2005).

[23] V. V. Konotop and M. Salerno, Phys. Rev. A **65**, 021602(R) (2002); V. A. Brazhnyi and V. V. Konotop, Mod. Phys. Lett. B **18**, 627 (2004).